Iraqi Journal of Science

ISSN: 0067-2904

Electrochemical Deposition of Hydroxyapatite Co-Substituted By Sr/Mg Coating on Ti-6Al-4V ELI Dental Alloy Post-MAO as Anti-Corrosion

Haider Abdulkareem AlMashhadani[1*], Khulood Abed Saleh[2]
[1]Al Rasheed University College, Dentistry Department, Baghdad, Iraq
[2]Department of Chem., College of Science, University of Baghdad, Jaderyah, Baghdad, Iraq

Received: 12/10/2019 Accepted: 30/12/2019

Abstract

This work involved the co-substitution of the two bioactive ions of strontium and magnesium into the hydroxyapatite (HA) coating which was then electrochemically deposited on Ti-6Al-4V ELI dental alloy (Gr.23) before and after treatment by Micro Arc Oxidation (MAO). The deposited layers were characterized by scanning electron microscopy (SEM), energy-dispersive X-ray spectroscopy (EDS), X-ray diffraction (XRD), and Fourier transform infrared spectroscopy (FTIR). The adhesion strength of the coating layer was estimated by using pull-off adhesion test. The adhesion strength of Sr/Mg-HA on the Ti-6Al-4V ELI dental alloy after MAO treatment was 1.79 MPa, which was higher than that before MAO treatment (1.62 MPa). The corrosion behavior of the alloy in artificial saliva environment at temperature ranged 293-323K was assessed by means of electrochemical techniques and potentiodynamic polarization curves. The corrosion protection to the alloy at 293K was increased from 67.98% before treatment by MAO to 75.87% after treatment. The antimicrobial properties of the coated alloy were evaluated against different bacteria and oral fungi (Candida).

Keywords: Hydroxyapatite, Dental alloy, Deposition, Corrosion, Titanium alloy.

الترسيب الكهروكيميائي لطلاء الهيدروكسي ابيتايت المعوض بأيوني السترونتيوم والمغنيسوم على سبيكة التيتانيوم السنية بعد المعالجة بواسطة (MAO) كمضاد للتآكل.

حيدر عبدالكريم المشهداني[1*], خلود عبد صالح[2]
[1]قسم طب الاسنان، كلية الرشيد الجامعة ، بغداد، العراق
[2]قسم الكيمياء، كلية العلوم، جامعة بغداد، بغداد، العراق

الخلاصة

في هذا البحث تم دراسة تأثير تعويض أيونين فعالين حيوياً وهما ايون السترونيتوم وايون المغنسيوم في طلاء الهيدروكسي ابيتايت وذلك بترسيبه على سبيكة التيتانوم نوع (Ti–6Al–4V ELI) قبل وبعد المعالجة بتقنية اكسدة القوس الدقيق (MAO) و بواسطة تقنية الترسيب الكهروكيميائي. تم تشخيص الطبقة المترسبة بواسطة المجهر الالكتروني الماسح و مطيافية تشتت الطاقة بالاشعة السينية وحيود الاشعة السينة و الاشعة تحت الحمراء. وتم فحص قوة الالتصاق لطبقة الطلاء على سبيكة التيتانوم بواسطة اختبار (Pull–off) وكانت قوة التصاق الطلاء على سبيكة التيتانوم المعالجة بواسطة (MAO) اعلى من قوة التصاق الطلاء على سبيكة التيتانوم قبل المعالجة بـ(MAO). وتم دراسة سلوك تآكل عينات التيتانوم قي محلول اللعاب المحضر

*Email: H_R200690@yahoo.com

مختبرياً عند مدى حراري 293 – 323 كلفن بمتابعة منحنيات الاستقطاب لتآكل سبيكة التيتانيوم وازدادت كفاءة حماية التآكل من 67,98% قبل المعالجة الى 75,87% بعد المعالجة بـ(MAO) وتم دراسة الفعالية البايلوجية ضد بكتريا مختلفة و فطريات الفم.

1. Introduction

Micro arc oxidation (MAO) is one of the most promising techniques for dental alloy surface therapy and has subsequently been widely accepted by multiple industry branches [1]. MAO is usually used on valve materials such as Al, Mg, Ti, Ta, Nb, Zr, and Be to create multi-purpose wear, anti-corrosion, heat-resistant dielectric, and ornamental coatings [1-4]. Titanium alloys are one of the most convenient bio-materials for dental applications because of low toxicity, superior corrosion resistance, good mechanical properties and biocompatibility with bone [5-7]. Due to the tendency of self healing it is deemed to have the highest bio-tolerance among all the currently used dental biomaterials [8].

Apatite can be deposited on dental implant surfaces because it is well accepted by living tissues, such as bone. Apatite can also promote strong bonds between tissues and dental implant surface [9, 10]. Hydroxyapatite (HA) is a valuable bone repair and regeneration material because of its compatibility to the inorganic phase of human bone [5].

HA has been widely used as a coating material for titanium dental implants in a variety of applications. Typically, the release of Ca^{2+} and PO_4^{3-} ions into the surrounding oral environment leads to the development of excellent interfacial strength between the implant and bone [11].

A wide range of different ions such as Sr, Zn, Ag, Mg, CO_3^{-2}, F and Si have been strategically incorporated into the structure of synthetic HA, replacing Ca/ PO_4^{3-}. The substitution of ions in HA modifies the crystallinity and crystal size and also changes material properties, namely thermal and phase stability, solubility, surface reactivity, and ability to be absorbed [12-14]. Sr plays a key role in bone bio-mineralization by promoting the number of osteoblasts and reducing the number and activity of osteoclasts. Sr is particularly useful in the treatment of osteoporosis [15]. Substitution of Mg into HA leads to improved cell growth, anti-corrosion, and an increase in bond strength compared to un-substituted HA coating. Mg-HA acts like Sr by improving the proliferation of osteoblast and inhibiting osteoclast activity. Incorporation Mg with HA decreases crystallinity and increases cell adhesion and bioactivity. Electrochemical deposition techniques were developed for the deposition of Sr/Mg-HA dispersed in a suitable solvent at a particular pH. These coatings require a MAO reaction to improve the coating properties [16, 17].

In this work, we investigated Sr/Mg-HA coating on Ti-6Al-4V ELI dental alloy by using electrochemical deposition before and after MAO treatment. The coatings were characterized by FTIR, X-ray and SEM. Coating adhesion was measured in order to assess their surface morphologies. The biological activities for the coating against several bacteria and oral fungi were also studied.

2. Experimental Part

2.1. Titanium Preparation

Circular shape samples of Ti-6Al-4V ELI dental alloys (Gr.23) were mechanically cut with dimensions of 1 cm diameter and 4-5 mm thickness.

These samples were polished with emery papers in different grades (600, 800, 1200 and 2000 mesh grit) successively washed with tap water, distilled water, ethanol, and acetone, and dried with a hair drier.

Before MAO treatment, the specimens were deoxidized by 10% NaOH then de-smutted by nitric acid 50%. After each step, they were double rinsed with distilled water and finally with acetone [18].

2.2. Artificial Saliva Preparation

The reference electrolyte used was the modified Fusayama artificial saliva, according to a previously described method [19], which closely resembles natural saliva. The composition of the artificial saliva is show in Table-1, while the pH of this electrolyte was 6.2 [19].

Table 1-The composition of the artificial saliva

	KCl	NaCl	$CaCl_2.H_2O$	$NaH_2PO_4.2H_2O$	$Na_2S.9H_2O$	urea
g/l	0.4	0.4	0.906	0.69	0.005	1

2.3. Micro Arc Oxidation of Ti alloys

For the MAO, an AC power of 150 V was applied for 120 sec. A titanium sample was used as an anode whereas a large titanium sheet was used as the cathode electrode in an electrolyte containing 10 g/L KH_2PO_4 and 0.5 g/L KOH. The electrolyte temperature was kept constant at 298 K. After the MAO, the samples were washed with distilled water and dried at room temperature. Figure-1 shows the structure of the MAO reaction cell.

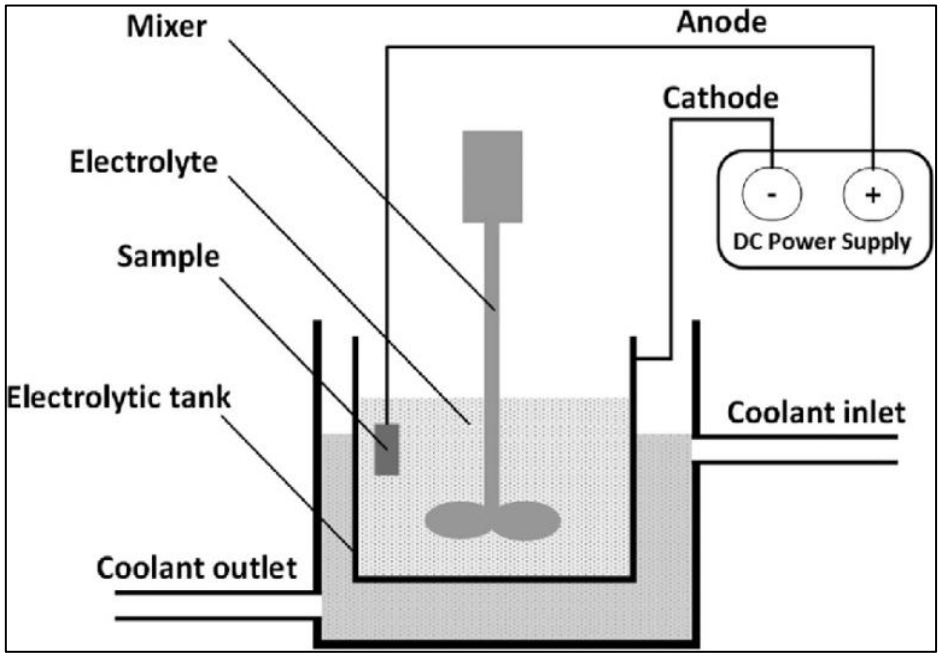

Figure 1-Micro Arc Oxidation cell [20]

2.4. Electrochemical deposition of Sr/Mg-HA

HA co-substituted with 5% Sr and 5% Mg was electrochemical deposited directly on the surface of a Gr.23 alloy. The experimental ratio of (Ca+x)/P (where x= Sr or Mg) was maintained at 1.7 (molar ratio). The suspension was prepared by dissolving calcium nitrate ($Ca(NO_3)_2$), strontium nitrate ($Sr(NO_3)_2$) and magnesium nitrate ($Mg(NO_3)_2$) in distilled water. Then, i-ammonium hydrogen phosphate ($(NH_4)_2HPO_4$) was added and the pH value of the solution was adjusted to 4.4 using dilute HNO_3. The electrochemical deposition of Sr/Mg-HA on Gr.23 was conducted at room temperature on a stirrer with direct current power (DC) (6 V), while the time was kept for 1 h. After deposition, the specimens were rinsed in distilled water, dried by a hair drier, and then soaked in 1 mol/L NaOH solution at 80 ^oC for 2 h

2.5. Characterization and test

Spectroscopic analysis of the formed Sr/Mg-HA coating was investigated with FT-IR. The surface morphologies of Sr/Mg-HA coating were measured and analyzed by XRD and SEM.

The galvanostatic polarization was measured using WENKING M Lab. device (Germany). Polarization curves were achieved for the corrosion of dental titanium alloys before and after MAO treatment. The obtained polarization curves involved the cathodic and anodic regions. Extensive data could be derived from the detailed analysis of each polarization region using an extrapolated method to determine both the corrosion current density (i_{corr}) and corrosion potential (E_{corr}).

The Sr/Mg-HA coating was tested for antimicrobial activity by well diffusion method against pathogenic bacteria such as *Gram-negative bacteria [Escherichia coli (E-coli) and Acinetobacter baumannii (A-baumannii)] and Gram-positive bacteria [Staphylococcus aureus (S-aureus) and Bacillus subtilis (B-subtilis)*], and oral fungi such as *Candida albicans (C-Albicans), Candida glabrata (C-glabrta), Candida parapsilosis (C-parapsiosis) and Candida tropicalis (C-tropicalis).*

3. Results and Discussion

3.1. Potentiostate polarization measurements

The effect of the coating layer on the polarization curves of Gr.23 corrosion was investigated in an artificial saliva solution, at a temperature range of 293-323K before and after MAO treatment (Figure-

2). The corrosion current density (i_{corr}) was determined by extrapolation Tafel lines. The results of the effects of Sr/Mg-HA coated layer on the corrosion parameters before and after MAO treatment are shown in Table-2.

It is clear from Figure-2 that E_{corr} for the uncoated and coated Gr.23 by Sr/Mg-HA before and after MAO treatment were shifted to a more active direction with increasing temperature from (293 to 323)K. E_{corr} for Gr.23 coated with Sr/Mg-HA before and after MAO treatment, at a temperature range of 293-323K, showed high values compared with the value for the uncoated Gr.23 alloy. Coating of Gr.23 by Sr/Mg-HA, before and after MAO treatment, led to increase E_{corr} values to the noble direction. This indicates that the titanium alloy is difficult to corrode after being coated by Sr/Mg-HA.

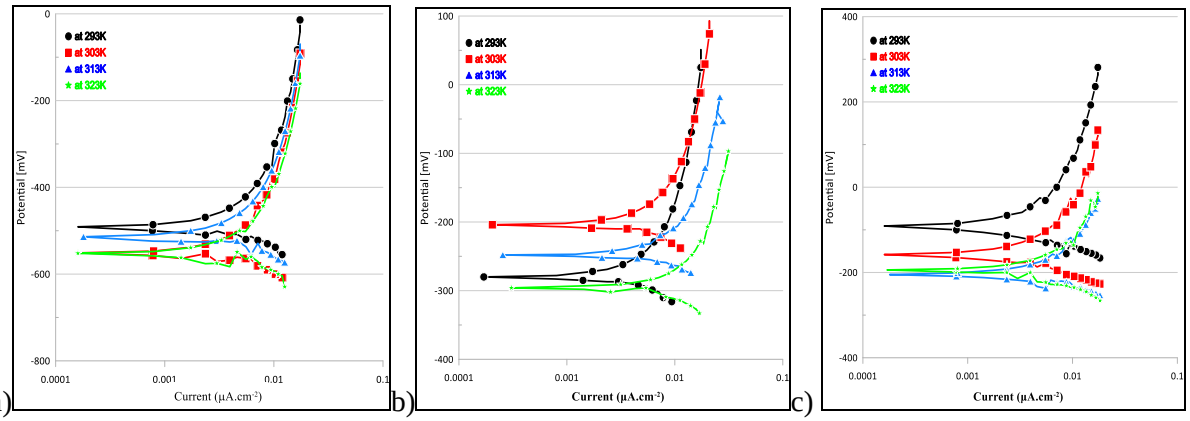

Figure 2-Polarization curves for Gr.23 a) Uncoated, b) Coated by Sr/Mg-HA before MAO and c) Coated by Sr/Mg-HA after MAO

Table 2-Corrosion parameters of coated Gr.23 before and after MAO treatment in artificial saliva at different Temperatures

Temp./K		E_{corr}/ mV	i_{corr}/µA. cm^{-2}	bc/mV. dec^{-1}	ba/mV. dec^{-1}	w.l/g. $m^{-2}.dl^{-1}$	P.L/ $mm.y^{-1}$	R_p / Ω.cm^2	PE%
Untreated	293	-490.5	3.030	102.4	285.5	0.324	0.0263	10800.64	-
	303	-551.2	3.490	106.1	391.9	0.374	0.0304	10388.23	-
	313	-515.9	3.800	158.0	400.2	0.412	0.0334	12943.94	-
	323	-550.6	3.820	135.3	495.8	0.516	0.0419	12082.27	-
Coated with Sr/Mg-HA	293	-281.0	0.970	11.2	42.6	0.104	0.0084	3969.90	67.98
	303	-204.4	1.110	12.8	46.9	0.120	0.0097	3933.61	68.19
	313	-248.5	1.580	19.6	54.2	0.169	0.0137	3955.92	58.42
	323	-295.9	1.760	63.2	53.5	0.189	0.0153	7148.14	53.92
Coated with Sr/Mg-HA after MAO	293	-92.1	0.731	41.3	56.5	0.078	0.0064	14172.56	75.87
	303	-158.3	0.873	38.1	56.6	0.094	0.0076	11326.17	74.98
	313	-204.9	0.910	33.2	40.0	0.098	0.0079	8656.68	76.05
	323	-193.7	0.974	38.9	42.1	0.104	0.0085	9013.51	74.50

The data in Table-2 show that i_{corr} values for Gr.23 coated by Sr/Mg-HA before MAO treatment are lower (0.97 to 1.76 µA.cm^{-2}) than those for uncoated Gr.23 (µA.cm^{-2} 3.03 to 3.82). Protection efficiency (PE %) was calculated using the following equation [21, 22]:

$$\%PE = \frac{(i_{corr})\mathrm{b} - (i_{corr})\mathrm{p}}{(i_{corr})\mathrm{b}} x\ 100 \qquad \ldots\ldots\ldots (1)$$

where (i_{corr})b and (i_{corr})p are the values of corrosion current density (µA.cm^{-2}) for uncoated and protected Gr.32, respectively.

This coating resulted in a protective layer against corrosion with a PE% value that reached to 67.98% at 293K. This protection was decreased with increasing temperature to reach to 53.92% at

323K. While coating the Gr.23 alloy with Sr/Mg-HA, after MAO treatment, led to a protective layer against temperature, where the PE% have was not effected by temperature and the PE% value ranged between 74.5 to 76.05% at temperature range of 293 to 323K.

Polarization near the corrosion potential E_{corr} was calculated to determine the polarization resistance on the basis of the following Stern–Geary equation [23, 24]:

$$R_p=\frac{\Delta E}{\Delta i}=\frac{b_a b_c}{2.303(b_a+b_a)}.\frac{1}{i_{corr}} \quad \ldots\ldots\ldots (2)$$

where R_p is the polarization resistance of the system, ΔE is the difference between the measured potential E and the corrosion potential E_{corr}, Δi is the difference between the measured current density i and the corrosion current density i_{corr} , and b_a and b_c are the anodic and cathodic Tafel coefficients, respectively.

The polarization resistance (R_p) for Gr.23 coated by Sr/Mg-HA, before MAO treatment, showed lower values compared with those for uncoated Gr.23. While coating by Sr/Mg-HA after MAO treatment caused an increase in R_p values at the temperature range of 293-303K, but the value was decreased with increasing temperature, as shown in Table-2.

3.2. Kinetic parameters for the corrosion process

The results of the corrosion kinetic parameters are listed in Table-3, Gr.23 coating by Sr/Mg-HA before and after MAO treatment caused an increase in E_a values from 6.0205 to 16.845 and 7.155 kJ.mol^{-1}, respectively. Figure-3 shows the values of logi$_{corr}$ plotted against reciprocal temperature for the corrosion of uncoated and coated Gr.23 by Sr/Mg-HA before and after MAO treatment.

Table 3-Kinetic and thermodynamic parameters for Gr.23 in artificial saliva at different temperatures in the range of 293-323K

	ΔG^* /kJ.mol^{-1}				ΔH^*/kJ. mol^{-1}	$-\Delta S^*$/ J.mol^{-1} .K^{-1}	Ea/kJ.mol^{-1}	A x10^{25} Molecules.cm^{-2} .S^{-1}
	293	303	313	323				
Uncoated	68.951	71.180	73.409	75.638	3.649	222.88	6.205	2.4
coated by Sr/Mg-HA before MAO	72.492	74.479	76.465	78.452	14.289	198.65	16.845	57.4
coated by Sr/Mg-HA after MAO	72.410	74.724	77.038	79.353	4.598	231.44	7.155	0.856

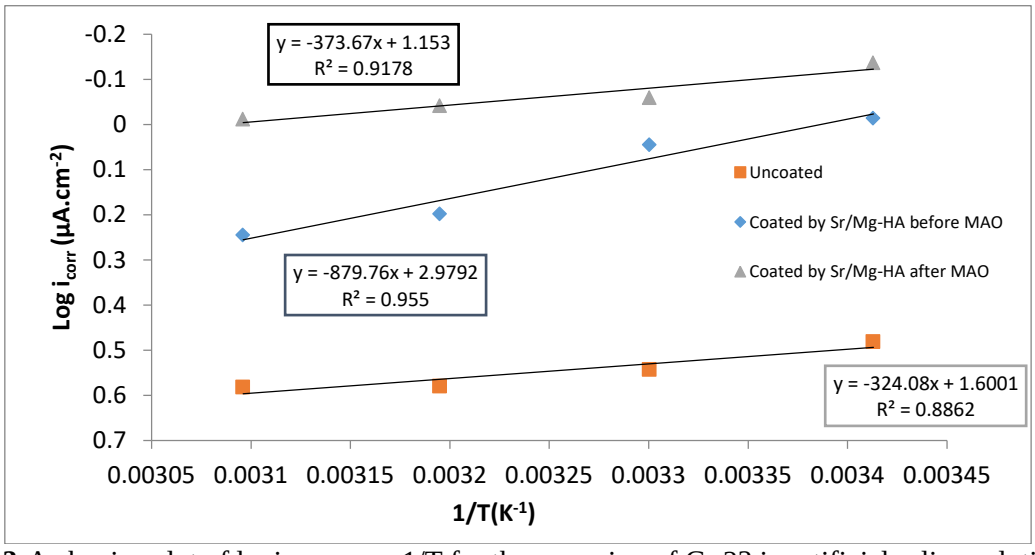

Figure 3-Arrhenius plot of logi$_{corr}$ versus 1/T for the corrosion of Gr.23 in artificial saliva solution.

The values of enthalpy of activation (ΔH*) and entropy of activation (ΔS*) are illustrated in Figure-4 as obtained by the transition state in eq.(3) [19]. ΔS* values, shown in Table-3, reflect the change in the order and transition state of orientation corrosion process of Gr.23. The data show slightly effected ΔS* values for Gr.23 coated by Sr/Mg-HA before and after MAO treatment.

$$log\frac{i_{corr}}{T} = log\frac{R}{Nh} + \frac{\Delta S^*}{2.303R} - \frac{\Delta H^*}{2.303RT} \quad \text{…….. (3)}$$

where i_{corr} is the corrosion current density of titanium in artificial saliva which is derived from Tafel plot, h is the Plank's constant, N is the Avogadro number , ΔS* is the activation entropy and ΔH* is the activation enthalpy. The plot of log i_{corr}/T against reciprocal temperature demonstrates straight lines with the slope of (-ΔH*/2.303 R) and an intercept of [(log(R/Nh)+(ΔS*/2.303R)], from which the values of ΔH* and ΔS* were calculated, respectively [19].

ΔH* is a component of activation energy, the values of which are linked to the values of E_a. The uncoated and coated Gr.23 before and after MAO treatment revealed an endothermic corrosion reaction with an increase in the value of enthalpy of activation. ΔG* showed positive values and almost a small change with increasing temperature, indicating that the activated complex was not stable and the probability of its formation decreased somewhat with rising temperature [25].

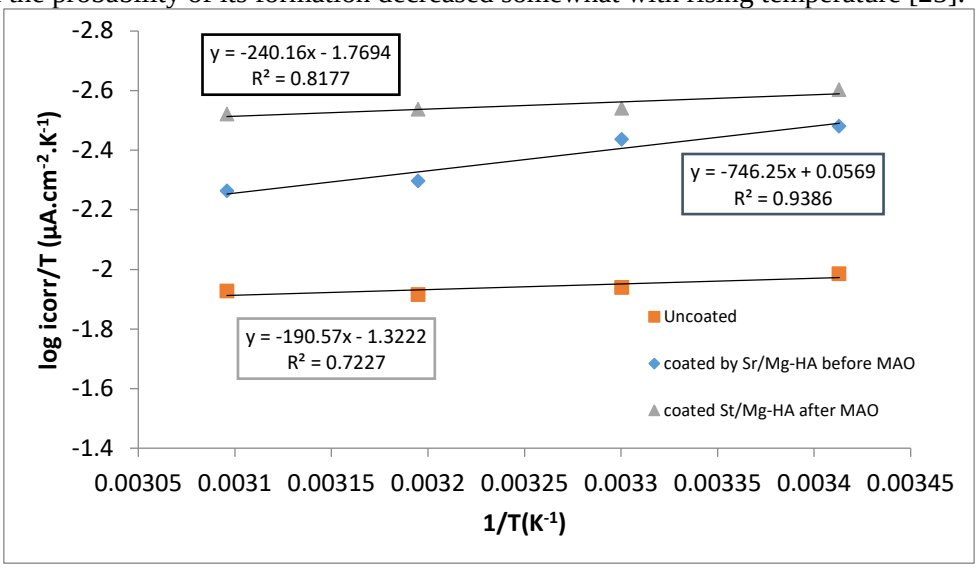

Figure 4-A plot of logi_{corr}/T Vs 1/T for the corrosion of Gr.23 in artificial saliva.

3.3. Chemical Structure and Morphology of Coating

SEM images showing surface morphologies for coated Gr.23 by Sr/Mg-HA before and after MAO treatment were analyzed (Figure-5), It is clear from Figure-(5a) that the coating was mainly continuous, uniform and composed of needle-like crystals. White spot-like Sr and Mg nanoparticles were sparsely dispersed in the coating, as proved by EDS point detection.

Figure-(5b) shows continuous, uniform and crack-free Sr/Mg-HA after MAO coating. This image demonstrates some globular and flake shape HA deposited in irregular manner on the surface of the Gr.23 after MAO. The average particles size of the coating was equal to 37.62 and 47nm before and after MAO treatment, respectively. The particles of Sr/Mg-HA deposited on the treated Gr.23 after MAO were larger than those before MAO. The size difference in the particles size of the coatings also indicated that the nucleation and growth conditions were different on the surface samples. The thickness of the coating was 3.62 µm, as revealed by the cross-sectional SEM micrograph shown in Figure-6.

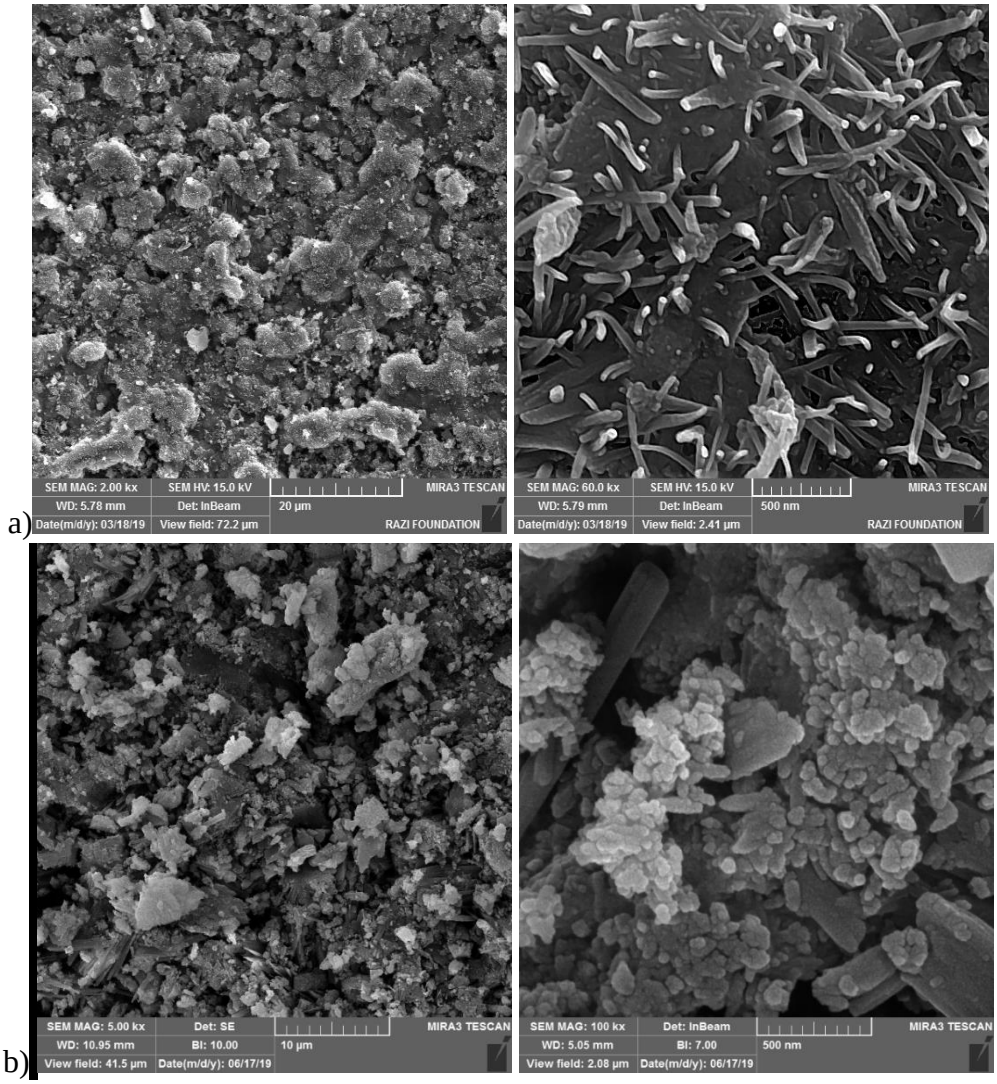

Figure 5-Scanning electron micrographs of Sr/Mg-HA deposited on Gr.23 (a) before and (b) after MAO treatment.

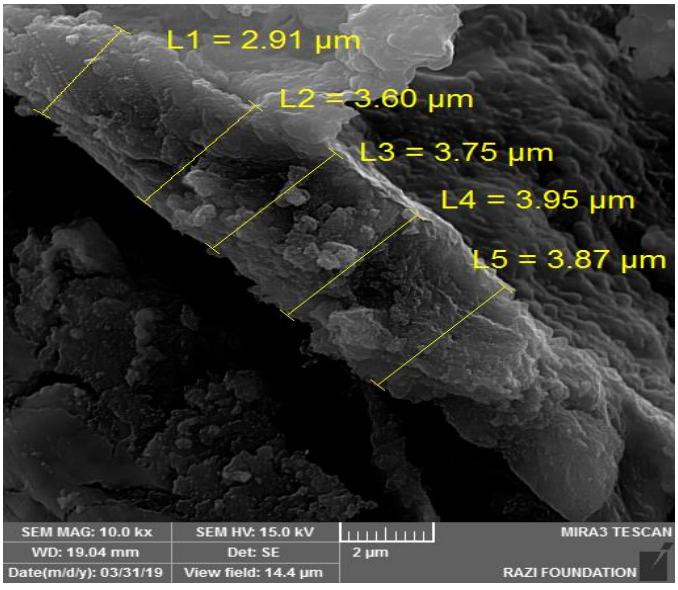

Figure 6-Cross section scanning electron micrographs of Sr/Mg-HA deposited on Gr.23 before MAO treatment.

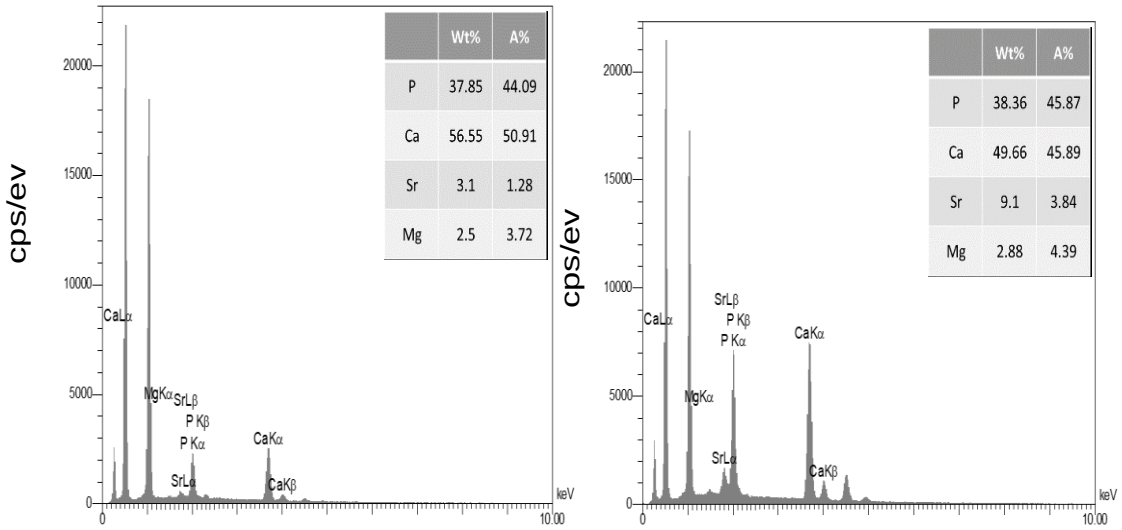

Figure 7-EDS spectra of Sr/Mg-HA coating on Gr.23 a)before and b)after MAO treatment.

The data in Figure-7 show that the values of the Ca/P ratio of HA and Sr/Mg-HA coating on Gr.23 before and after MAO treatment were 1.15 and 1, respectively, which were remarkably lower than the expected ratio. The observed percentages of Sr and Mg ions were higher in Gr.23 coated by Sr/Mg-HA after MAO than those before MAO treatment. This might suggest the incorporation of Sr and Mg ions in the porous structure on the surface of titanium as a result of MAO treatment.

XRD patterns of the Sr/Mg-HA coatings are shown in Figure-8. The peaks of titanium are evident in all the patterns. The overall diffraction patterns are in agreement with those reported by the current literature [26-29], showing the characteristic peaks of HA [28]. The pattern for Gr.23 coated with Sr/Mg-HA after MAO is less intense and experienced a slight shift when compared with the coated alloy after MAO.

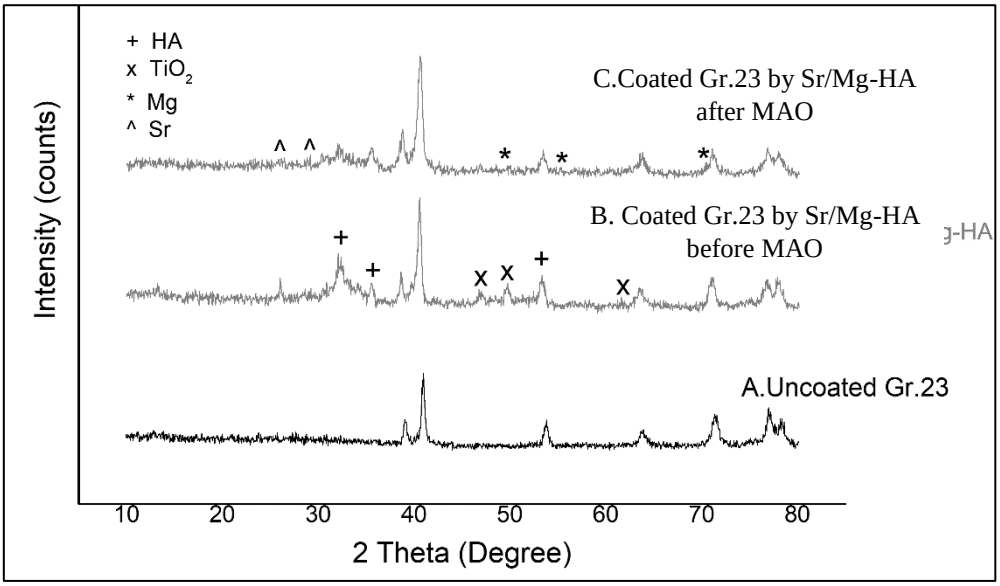

Figure 8-XRD pattern of Gr.23; (A) uncoated, (B) coated by Sr/Mg-HA before MAO, and (C) coated by Sr/Mg-HA after MAO.

FT-IR was used as a complementary technique to XRD and EDS analyses and confirmed the chemical changes in HA after the addition of ions. FT-IR spectra for the Sr/Mg-HA coatings as dried powders, presented in Figure-9, indicated the vibrational modes of PO_4 groups at 499, 526, 987 and 1060-1134 cm^{-1} and an OH group at 638 cm^{-1} (Librational mode, νL, of hydroxyl groups OH^-) [30] and 3492, 3544at cm^{-1} (Stretching mode, νs, of hydroxyl groups OH^-) [31] of the apatite phase for the

coated powder [32]. The presence of adsorbed water could also be detected from FT-IR spectra in the region around 3188–3402 cm^{-1} [32].

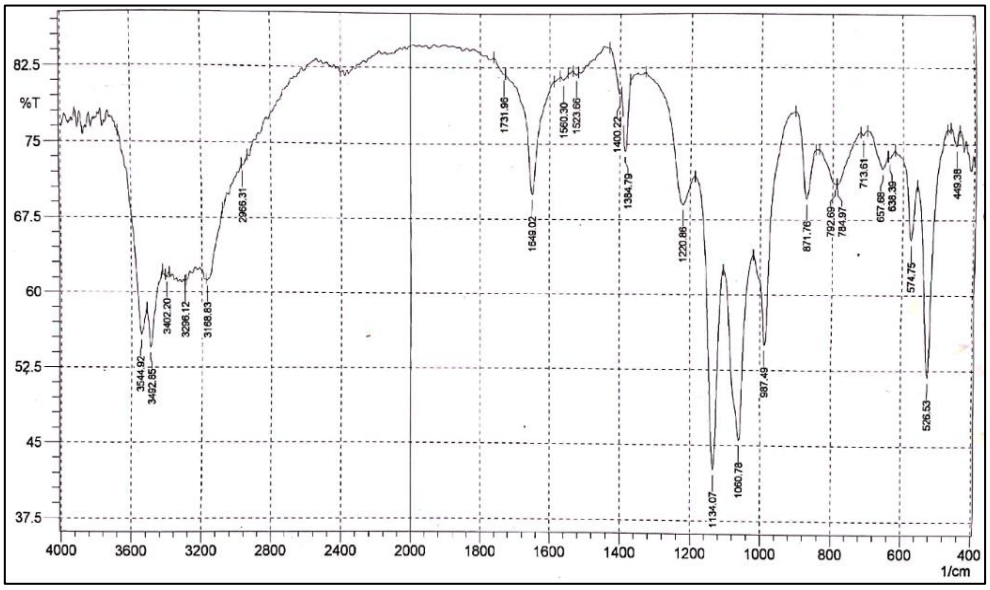

Figure 9-FT-IR spectra for coating of Sr/Mg-HA.

3.4. Adhesion Test

Excellent adhesion of a Sr/Mg-HA coated film on the Ti surface led to good corrosion protection for Ti alloy. Adhesion testing determines how well a coating is bonded to the Ti surface. The adhesion pull-off testing was performed for different coating types.

The values for the failure strength and the type of failure indicated that the Sr/Mg-HA coating after MAO treatment reached to 1.61 MPa, which revealed stronger adhesive properties those of the coating before MAO treatment (1.79 MPa).

3.5. Antimicrobial Activity

With the expanding rate of microbial species in the oral cavity which are becoming resistant to present antibiotics, many studies have attempted to provide effective antimicrobial agents with low cost. Such problems have led to the resurgence in the use of metal-based antiseptics which are applicable to broader spectrum of bacteria, with far lower susceptibility to induce resistance than common antibiotics.

The results of the antibacterial activity of Sr/Mg-HA coating against different bacteria are listed in Table-4. The positive control, using amoxicillin treatment, was highly effective against Gram- positive bacteria, with a lower effectiveness against Gram- negative bacteria, at 1 mg/mL concentration. The negative control treatment with DMSO did not have any activity against both Gram-positive and negative bacteria. The highest antibacterial activity for Sr/Mg-HA coating was observed against *B. subtilis* , followed by activity against *S. aureus.* The antibacterial activities of Sr/Mg-HA coating against *E. coli* and *A. baumannii* were similar to that of the positive control, as shown in Table-4.

Table 4-Antibacterial activity (zone of inhibition, mm) of the Sr/Mg-HA coating

	E.Coli	**A. baumannii**	**B.subtilis**	**S. aureus**
Amoxicillin (+ve)	13	14	31	25
Sr/Mg-HA coating	13	13	29	27

Table-5 shows the antifungal activity of Sr/Mg-HA coating. The positive control, represented by Fluconazole treatment, was highly effective against *Candida* species at the concentration of 1 mg/ml. The antifungal activity of the coating was tested against four *Candida* species (*C. albicans, C. tropicalis, C. glabrata*, and *C. parapsilosis*) by well diffusion method. The inhibition zone was observed in Sr/Mg-HA coating against *C. albicans* and *C. glabrata*, while no antifungal activity was observed against *C. tropicalis* and *C. parapsilosis*, as shown in Table-5.

Table 5-Antifungal activity (zone of inhibition, mm) of the Sr/Mg-HA coating

	C. albicans	*C. tropicalis*	*C. glabrata*	*C. parapsilosis*
Fluconazole (+ve)	28	22	22	22
Sr/Mg-HA coating	16	-	16	-

4. Conclusions

Electrochemical deposition of Sr/Mg-HA coating on Ti-6Al-4V ELI dental alloy (Gr.23) after MAO treatment increased the corrosion efficiency from 67.98 to 75.87 % at 293K compared with that before MAO treatment. The particle size of Sr/Mg-HA deposited on the treated Gr.23 by MAO was larger than that before MAO treatment. The size difference of the particles of coating also indicated that the nucleation and growth conditions were different on the surface samples.

The adhesion strength of Sr/Mg-HA on Gr.23 was increased when coated on a surface treated by MAO. The antibacterial activity of Sr/Mg-HA coating was higher against Gram-positive bacteria than that against Gram-negative bacteria. The antifungal activity of Sr/Mg-HA coating showed activity against *C. albicans* and *C. glabrata* species, with no activity against *C. tropicalis* and *C. parapsilosis* species.

References

1. Fei, C., Hai, Z., Chen, C. and Yangjian, X. **2009**. "Study on the tribological performance of ceramic coatings on titanium alloy surfaces obtained through microarc oxidation," *Progress in Organic Coatings*, **64**: 264-267.
2. Santos-Coquillat, A., Tenorio, R.G., Mohedano, M., Martinez-Campos, E., Arrabal, R. and Matykina, E. **2018**. "Tailoring of antibacterial and osteogenic properties of Ti6Al4V by plasma electrolytic oxidation," *Applied Surface Science*, **454**: 157-172.
3. Wang, Y., Jiang, B., Lei, T. and Guo, L. **2004**. "Dependence of growth features of microarc oxidation coatings of titanium alloy on control modes of alternate pulse," *Materials Letters*, **58**:1907-1911.
4. Yerokhin, A., Nie, X., Leyland, A. and Matthews, A. **2000**. "Characterisation of oxide films produced by plasma electrolytic oxidation of a Ti–6Al–4V alloy," *Surface and Coatings Technology*, 130:195-206.
5. Rautray, T.R., Narayanan, R., Kwon, T.Y. and Kim, K.H. **2010**. "Surface modification of titanium and titanium alloys by ion implantation," *Journal of Biomedical Materials Research Part B: Applied Biomaterials*, **93**: 581-591.
6. Rautray,T. R. Mohapatra, B. and Kim., K.-H. **2014**. "Fabrication of strontium–hydroxyapatite scaffolds for biomedical applications," *Advanced Science Letters*, **20**: 879-881.
7. Wang,Y. Wen, C. Hodgson, P. and Li.,Y. **2014**."Biocompatibility of TiO2 nanotubes with different topographies," *Journal of Biomedical Materials Research Part A*, **102**: 743-751.
8. W. Simka, A. Sadkowski, M. Warczak, A. Iwaniak, G. Dercz, J. Michalska, *et al.* , **2011**, "Characterization of passive films formed on titanium during anodic oxidation," *Electrochimica Acta*, **56**: 8962-8968.
9. S. Sobieszczyk and R. Klotzke. **2011**. "Nanotubular titanium oxide layers for enhancement of bone-implant bonding and bioactivity," *Advances in Materials Sciences*, **11**: 17-26.
10. T. R. Rautray, R. Narayanan, T.-Y. Kwon, and K.-H. Kim. **2010**. "Accelerator based synthesis of hydroxyapatite by MeV ion implantation," *Thin Solid Films*, **518**: 3160-3163.
11. K. Raja, G. Craviso, M. Misra, A. Raichur, and A. Kar. **2008**. "Development of Novel Biocompatible Hydroxyapatite Coated Nanotubular Titania for Implant Application," *Advances in Bioceramics and Porous Ceramics: Ceramic Engineering and Science Proceedings*, **29**(7)*:* 227-237.
12. S. C. Cox, P. Jamshidi, L. M. Grover, and K. K. Mallick. **2014**. "Preparation and characterisation of nanophase Sr, Mg, and Zn substituted hydroxyapatite by aqueous precipitation," *Materials Science and Engineering: C*, **35**: 106-114.
13. V. Aina, L. Bergandi, G. Lusvardi, G. Malavasi, F. E. Imrie, I. R. Gibson, *et al.* . **2013**. "Sr-containing hydroxyapatite: morphologies of HA crystals and bioactivity on osteoblast cells," *Materials Science and Engineering: C*, **33**: 1132-1142.

14. S. Aryal, K. Matsunaga, and W.-Y. Ching. **2015**. "Ab initio simulation of elastic and mechanical properties of Zn-and Mg-doped hydroxyapatite (HAP)," *Journal of the mechanical behavior of biomedical materials,* **47**: 135-146.

15. M. Kavitha, R. Subramanian, R. Narayanan, and V. Udhayabanu. **2014**, "Solution combustion synthesis and characterization of strontium substituted hydroxyapatite nanocrystals," *Powder technology,* **253**: 129-137.

16. A. Farzadi, F. Bakhshi, M. Solati-Hashjin, M. Asadi-Eydivand, and N. A. abu Osman. **2014**. "Magnesium incorporated hydroxyapatite: Synthesis and structural properties characterization," *Ceramics International,* **40**: 6021-6029.

17. Y. Yajing, D. Qiongqiong, H. Yong, S. Han, and X. Pang, **2014**, "Magnesium substituted hydroxyapatite coating on titanium with nanotublar TiO2 intermediate layer via electrochemical deposition," *Applied Surface Science,* **305**: 77-85.

18. S. Meyer, R. Gorges, and G. Kreisel. **2004**. "Preparation and characterisation of titanium dioxide films for catalytic applications generated by anodic spark deposition," *Thin Solid Films,* **450**: 276-281.

19. K. A. S. Al-Saadie and H. A. Y. AlMashhadani. **2019**. "Corrosion Protection of Pure Titanium Implant by Electrochemical Deposition of Hydroxyapatite Post-Anodizing," in *IOP Conf. Series: Materials Science and Engineering*, 12071.

20. M. Z. Ibrahim, A. A. Sarhan, F. Yusuf, and M. Hamdi. **2017**. "Biomedical materials and techniques to improve the tribological, mechanical and biomedical properties of orthopedic implants–A review article," *Journal of Alloys and Compounds,* **714**: 636-667.

21. H. A. Abbas, K. A. S. Alsaade, and H. A. Y. AlMAshhdani. **2019**. "Study the Effect of Cyperus Rotundus Extracted as Mouthwash on the Corrosion of Dental Amalgam," in *IOP Conference Series: Materials Science and Engineering*, 012074.

22. S. Shivakumar and K. Mohana, **2013**, "Studies on the inhibitive performance of Cinnamomum zeylanicum extracts on the corrosion of mild steel in hydrochloric acid and sulphuric acid media," *Journal of Materials and Environmental Science,* **4**: 448-459.

23. M. Schorr and J. Yahalom. **1972**. "The significance of the energy of activation for the dissolution reaction of metal in acids," *Corrosion Science,* **12**: 867-868.

24. K. A. S. Al-Saadie and H. A. Y. Al-Mashhdani. **2015**. "Corrosion Protection Study for Caron Steel in Seawater by Coating with SiC and ZrO 2 Nanoparticles," *American Journal of Chemistry,* **5**: 28-39.

25. R. A. Mohammed. **2014**. "An investigation of electropolymerization and corrosion protection properties of polypyrrole coating on carbon steel and stainless steel," Msc, Chemistry, University of Baghdad, Iraq.

26. I. Smičiklas, A. Onjia, and S. Raičević. **2005**. "Experimental design approach in the synthesis of hydroxyapatite by neutralization method," *Separation and Purification Technology,* **44**: 97-102.

27. M. H. Santos, M. d. Oliveira, L. P. d. F. Souza, H. S. Mansur, and W. L. Vasconcelos, **2004**, "Synthesis control and characterization of hydroxyapatite prepared by wet precipitation process," *Materials Research,* **7**: 625-630.

28. S. Koutsopoulos, "Synthesis and characterization of hydroxyapatite crystals: a review study on the analytical methods. **2002**." *Journal of Biomedical Materials Research: An Official Journal of The Society for Biomaterials, The Japanese Society for Biomaterials, and The Australian Society for Biomaterials and the Korean Society for Biomaterials,* **62**: 600-612.

29. S. Kweh, K. Khor, and P. Cheang. **1999**. "The production and characterization of hydroxyapatite (HA) powders," *Journal of Materials Processing Technology,* **89**: 373-377.

30. J. Arends, J. Christoffersen, M. Christoffersen, H. Eckert, B. Fowler, J. Heughebaert, *et al.* . **1987**. "A calcium hydroxyapatite precipitated from an aqueous solution: an international multimethod analysis," *Journal of Crystal Growth,* **84**: 515-532.

31. F. Freund and R. M. Knobel. **1977**. "Distribution of fluorine in hydroxyapatite studied by infrared spectroscopy," *Journal of the Chemical Society, Dalton Transactions,* 1136-1140.

32. D. Laurencin, N. Almora-Barrios, N. H. de Leeuw, C. Gervais, C. Bonhomme, F. Mauri, *et al.* .**2011**. "Magnesium incorporation into hydroxyapatite," *Biomaterials,* **32**: 1826-1837.